Inorg. Chem. **XXXX**, *xx*, 0

Preparation and Crystal Structures of Bismuth Technetates: A New Metal Oxide System

Efrain E. Rodriguez,[†,‡] Frédéric Poineau,[§] Anna Llobet,[†] Ken Czerwinski,[§] Ram Seshadri,[‡] and Anthony K. Cheetham*[,||]

Manuel Lujan Neutron Scattering Center, Los Alamos National Laboratory, Los Alamos, New Mexico 87545, Materials Research Laboratory, University of California, Santa Barbara, California 93106, Harry Reid Center for Environmental Studies, University of Nevada, Las Vegas, Nevada 89154-4009, and Department of Materials Science and Metallurgy, University of Cambridge, Pembroke Street, Cambridge, CB2 3QZ, U.K.

Received February 21, 2008

Two new oxides have been unambiguously identified as $Bi_2Tc_2O_{7-\delta}$ with $\delta = 0.14(1)$ and Bi_3TcO_8 through X-ray absorption near-edge structure spectroscopy and neutron powder diffraction. The compound $Bi_2Tc_2O_{7-\delta}$ has a cubic pyrochlore-type structure with $a = 10.4746(1)$ Å, space group $Fd\bar{3}m$ (origin choice 2), and $Z = 8$. The compound Bi_3TcO_8 is also cubic, $a = 11.5749(1)$ Å, space group $P2_13$, $Z = 8$, and has a fluorite-related crystal structure. In $Bi_2Tc_2O_{7-\delta}$ the Tc(IV) cations are octahedrally coordinated, whereas in Bi_3TcO_8 the Tc(VII) cations are tetrahedrally coordinated. A third new phase, probably $Bi_3Tc_3O_{11}$, could not be obtained pure, but preliminary X-ray powder diffraction data affords a primitive cubic lattice with $a = 9.3433(1)$ Å. On the basis of structural similarities between $Bi_2Tc_2O_{7-\delta}$ and closely related oxides, $Bi_2Tc_2O_{7-\delta}$ is expected to be a metallic oxide with Pauli paramagnetism. Electronic structure calculations of both $Bi_2Tc_2O_{7-\delta}$ and Bi_3TcO_8 further support metallic conductivity in the former and insulating behavior in the latter. The inert pair effect of the Bi cations on the crystal structures of $Bi_2Tc_2O_{7-\delta}$ and Bi_3TcO_8 is also described. In addition, calculations of the valence electron localization function for $Bi_2Tc_2O_{7-\delta}$ and Bi_3TcO_8 provide further visualization of the Bi $6s^2$ lone pair electrons in the real space of the crystal structures.

1. Introduction

Located at the center of the transition element series, technetium is the lightest radioelement of the periodic table. The long-lived isotope ^{99}Tc ($t_{1/2} = 2.13 \times 10^5$ yrs, $\beta^- = 0.29$ MeV) is produced in large quantities from spent nuclear fuel (up to 6% yield) and decays to stable ruthenium-99.[1] The long half-life, high yield in the nuclear fuel cycle, and affinity to form the highly mobile pertechnetate species make ^{99}Tc a unique challenge to safe disposal of nuclear waste.[2–4] Exploring the solid-state chemistry of ternary Tc oxides could lead to a potentially robust waste form. In addition, such studies may also promote special applications for the otherwise unwanted isotope.

Excluding the salts of the TcO_4^- anion, studies of ternary Tc oxides have not been undertaken in nearly 40 years.[5,6] Furthermore, ternary oxides of Tc with a post transition element were never pursued with the exception of the compound $PbTcO_3$.[5] Mixed-metal systems combining transition metals with heavy main group elements such as mercury, thallium, lead, and bismuth can lead to interesting materials properties. For example, the often stereochemically active $6s^2$ electrons of Tl^+, Pb^{2+}, and Bi^{3+} can lead to polar behavior including ferroelectricity. Also, mixed-metal oxides of neighboring metal ruthenium with either bismuth or lead have been investigated for use as electro-catalysts for the reduction

* To whom correspondence should be addressed. akc30@cam.ac.uk.
† Los Alamos National Laboratory.
‡ University of California.
§ University of Nevada.
|| University of Cambridge.

(1) Schwochau, K. *Technetium: Chemistry and Radiopharmaceutical Applications*; Wiley-VCH: Weinheim, Germany, 2000.
(2) Lieser, K. H. *Radiochim. Acta* **1993**, *63*, 5–8.
(3) Maes, A.; Geraedts, K.; Bruggeman, C.; Vancluysen, J.; Rossberg, A.; Hennig, C. *Environ. Sci. Technol.* **2004**, *38*, 2044–2051.
(4) Lukens, W. W.; Bucher, J. J.; Edelstein, N. M.; Shuh, D. K. *Environ. Sci. Technol.* **2002**, *36*, 1124–1129.
(5) Muller, O.; White, W. B.; Roy, R. *Inorg. Nucl. Chem.* **1964**, *26*, 2075–2085.
(6) Keller, V. C.; Wassilopulos, M. *Radiochim. Acta* **1966**, *5*, 87–91.

10.1021/ic8003273 CCC: $40.75
Published on Web 06/24/2008

and evolution of oxygen[7–9] and as cathodes in solid oxide fuel cells.[10,11] Therefore, our first study of a new Tc ternary system is focused on Bi-containing oxides.

Because the chemistry of Tc broadly resembles that of its heavier congener rhenium,[12,13] it was expected that the Bi−Tc−O system would include similar phases observed in the Bi−Re−O system. Through the reaction of Bi_2O_3 and Re oxides, a host of new phases were prepared with a diverse array of crystal structure types and Re in various oxidation states.[14–16] However, the oxide chemistry of Tc(IV) can occasionally resemble that of Ru(IV) more closely than that of Re(IV). For example, several Tc(IV) ternary oxides are isostructural to Ru(IV) ternary oxides such as lanthanide-containing pyrochlores[5,17] and alkali metal-containing perovskites.[6] Indeed, the current investigation led to the preparation of Bi−Tc−O phases similar to those in both the Bi−Ru−O and Bi−Re−O systems.

We recently reported the crystal structure and electronic properties of TcO_2.[18] In the present work, we report the preparation of two new ternary oxides, $Bi_2Tc_2O_7$ and Bi_3TcO_8, in a metal oxide system never before studied. We also report the crystal structures of these new oxides along with their calculated electronic band structures and evaluate how the stereochemical activity of the Bi lone pair electrons is manifested in each. Finally, we discuss, on the basis of the structural information and known properties of closely related oxides, the possible materials properties of the bismuth technetates.

2. Experimental and Computational Details

2.1. Sample Preparation. ***Caution!*** *^{99}Tc is radioactive with a specific activity of 17 mCi/gram. To prevent contamination and ensure personal safety, all preparations were performed in a fume hood. A polycarbonate shield with a thickness of 1 cm was used when manipulating the powders. In addition, standard practices of a radiochemistry laboratory must be followed.*

The $Bi_2Tc_2O_7$ phase was prepared by heating a stoichiometric mixture of Bi_2O_3 and TcO_2 at 700 °C in a fused quartz boat under flowing Ar gas. The Bi_2O_3 was obtained from Sigma-Aldrich (99.999% purity), and TcO_2 was prepared by thermal decomposition of freshly crystallized, white NH_4TcO_4 as described previously.[18] Mixtures were combined in a mortar and pestle as slurries with methanol. The heating of several nonstoichiometric mixtures at 700 °C always produced the $Bi_2Tc_2O_7$ phase with some residual Bi_2O_3 and TcO_2. When stoichiometric mixtures were heated above 800 °C in an evacuated quartz ampoule or at 700 °C under an argon atmosphere, the $Bi_2Tc_2O_7$ phase was obtained without impurities. The powder has a dark-gray color.

By combining $Bi_2Tc_2O_7$ with a stoichiometric amount of Bi_2O_3 and heating the mixture in dry O_2 gas, Bi_3TcO_8 was prepared. The starting materials were ground as slurries with methanol, and the dry mixture transferred into a pyrex tube. Approximately two atmospheres of dry O_2 gas and 200 mg of the powder mixture in the pyrex ampoule were heated to 450 °C in a tube furnace with flowing argon gas (in case of a leak) for four hours. Afterward, the ampoule was furnace cooled and the powder mixture appeared a pale-yellow color. A third phase believed to be $Bi_3Tc_3O_{11}$ could not be obtained monophasically. Apparently, it is a low-temperature phase because it was formed by heating Bi_2O_3 and TcO_2 powders at 550 °C for 8 h under flowing argon gas, which produced the $Bi_2Tc_2O_7$ and $Bi_3Tc_3O_{11}$ phases. When an ampoule of the powder mixture with a low O_2 partial pressure was heated to 450 °C, the resulting powder was a combination of Bi_3TcO_8 and $Bi_3Tc_3O_{11}$.

2.2. Characterization. X-ray diffraction (XRD) powder patterns of the new phases were qualitatively indexed with the lattice parameters of closely related oxides. Silicon powder 640c obtained from the National Institute of Standards was used as an internal standard to precisely determine the lattice parameters.

To qualitatively determine the local environment around the technetium cations, X-ray absorption near-edge structure (XANES) spectroscopy was performed on the $Bi_2Tc_2O_7$ and Bi_3TcO_8 powders. For the sample preparation, thin films of the samples with epoxy between two Capton films (25 μm) were mounted onto stainless-steel holders. The XANES experiments were performed at the Advanced Photon Source at Argonne National Laboratories. Beamline ID-10 in the MR-CAT sector was used for the Bi_3TcO_8 measurement and for the $Bi_2Tc_2O_7$ sample, beamline 12-BM in the BSSRC sector. For $Bi_2Tc_2O_7$, the data was collected in fluorescence mode and for Bi_3TcO_8 in transmission mode. For both, the energy was tuned with technetium metal (K-edge energy = 21.044 keV). During the $Bi_2Tc_2O_7$ experiment, the spectrum of TcO_2 was also measured as a reference.

For the neutron powder diffraction (NPD) measurements, approximately 880 mg of the $Bi_2Tc_2O_7$ product were transferred into a vanadium sample holder inside a glovebag filled with helium. Similarly, 850 mg of Bi_3TcO_8 were loaded into a vanadium can. The NPD patterns for both samples were collected with the high-intensity powder diffractometer HIPD at the Manuel Lujan Neutron Scattering Center at the Los Alamos Neutron Science Center (LANSCE). For the Bi_3TcO_8 sample, the high-resolution powder diffractometer NPDF at LANSCE was also employed. NPD measurements were performed at temperatures between 15 and 300 K on HIPD and NPDF. The neutrons were collected in time-of-flight mode with various detector banks covering a *d*-spacing range of 0.4−40 Å for HIPD and 0.12−7.2 Å for NPDF.

2.3. Electronic Structure Calculations. To investigate the electronic band structure of $Bi_2Tc_2O_7$ and Bi_3TcO_8, linear muffin-tin orbital (LMTO) calculations[19,20] were performed within the atomic sphere approximation. The scalar-relativistic Kohn−Sham equations were solved within the local-density approximation.[21] In addition, all relativistic effects were taken into account except for spin−orbit coupling. For $Bi_2Tc_2O_7$, the calculations were

(7) Horowitz, H. S.; Longo, J. M.; Lewandowski, J. T., U.S. Patent 4,146,458 , 1979.
(8) Horowitz, H. S.; Longo, J. M.; Horowitz, H. H. *J. Electrochem. Soc.* **1983**, *130*, 1851–1859.
(9) Gökaaç, G.; Kennedy, B. J. *Langmuir* **1993**, *9*, 1862–1867.
(10) Esposito, V.; Luong, B. H.; Di Bartolomeo, E.; Wachsman, E.; Traversa, E. *J. Electrochem. Soc.* **2006**, *153*, A2232–A2238.
(11) Takeda, T.; Kanno, R.; Kawamoto, Y.; Takeda, Y.; Yamamoto, O. *J. Electrochem. Soc.* **2000**, *147*, 1730–1733.
(12) Peacock, R. D. *The Chemistry of Technetium and Rhenium*; Elsevier: New York, 1966.
(13) Colton, R. *The Chemistry of Rhenium and Technetium*; Interscience Publishers (Wiley): New York, 1965.
(14) Rae-Smith, A. R.; Cheetham, A. K. *J. Solid State Chem.* **1979**, *30*, 345–352.
(15) Cheetham, A. K.; Rae-Smith, A. R. *Mater. Res. Bull.* **1981**, *16*, 7–14.
(16) Cheetham, A. K.; Rae-Smith, A. R. *Acta Crystallogr.* **1985**, *B41*, 225–230.
(17) Muller, O. Ph.D. Thesis, Pennsylvania State Univesity, 1968.
(18) Rodriguez, E. E.; Poineau, F.; Llobet, A.; Sattelberger, A. P.; Bhattacharjee, J.; Waghmare, U. V.; Hartmann, T.; Cheetham, A. K. *J. Am. Chem. Soc.* **2007**, *129*, 10244–10248.
(19) Andersen, O. K. *Phys. Rev. B* **1975**, *12*, 3060.
(20) Jepsen, O.; Andersen, O. K. *Z. Phys. B* **1995**, *97*, 35.
(21) von Barth, U.; Hedin, L. *J. Phys. C.* **1972**, *5*, 1629.

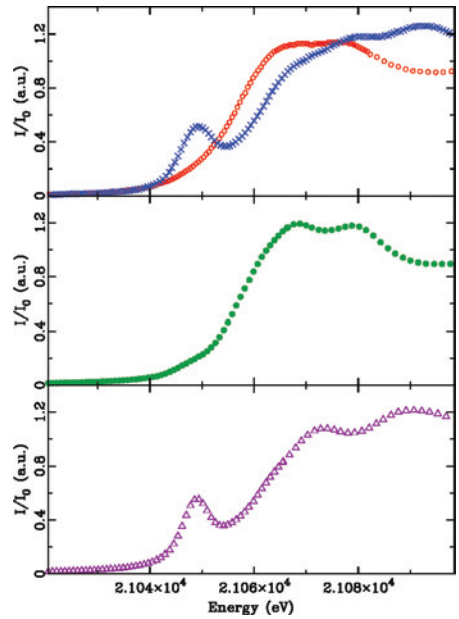

Figure 1. XANES spectra for the $Bi_2Tc_2O_7$ (○), Bi_3TcO_8 (×), TcO_2 (•), and NH_4TcO_4 (△). The NH_4TcO_4 spectrum was taken from previous work.[27]

performed on 256 irreducible k points within the primitive wedge of the Brillouin zone, and 12 irreducible k points for Bi_3TcO_8 because it has a much larger cell. The crystal structures reported in the Results section were used for the calculations. To map in real space the core, bonding, and nonbonding regions of the crystal structures, the LMTO electronic structures were analyzed by calculating the electron localization function (ELF),[22,23] in a similar fashion employed in an earlier study of Bi-containing oxides.[24] The *Stuttgart TB-LMTO-ASA* program (version 47C) was used for all of the computational work.[25]

3. Results

3.1. X-ray Absorption Near-Edge Structure. XANES spectroscopy is commonly used for characterization of the local geometry and oxidation state of absorbing atoms. The XANES spectra collected for Bi_3TcO_8, $Bi_2Tc_2O_7$, and TcO_2 were background subtracted and normalized using the *ATHENA* software.[26] The normalized spectra of Bi_3TcO_8, $Bi_2Tc_2O_7$, TcO_2, and NH_4TcO_4, which were obtained from previous work,[27] are presented in Figure 1. The shift to a higher energy of the technetium K-edge in Bi_3TcO_8 relative to that of $Bi_2Tc_2O_7$ indicates a higher oxidation state for technetium in the former.

Another notable difference between the two XANES spectra is the pre-edge feature observed in Bi_3TcO_8 but not in $Bi_2Tc_2O_7$. The pre-edge feature in Bi_3TcO_8 is qualitatively similar to that observed in pertechnetate salts such as NH_4TcO_4 (Figure 1). This feature is observed for the TcO_4^- anion due to an electronic transition (s → p) in tetrahedral and square pyramidal species.[28] In centrosymmetric molecules, the pre-edge feature is not observed because the electronic transition with this geometry (s → d) is forbidden. Therefore, the technetium cation must be centrosymmetric, either octahedral or trigonal, in $Bi_2Tc_2O_7$ and tetrahedral in Bi_3TcO_8. The neutron diffraction results provide a more quantitative description of the local geometries.

Table 1. Structural Parameters with Standard Uncertainties Shown in Parentheses for the $Bi_2Tc_2O_7$ Phase, Space Group $Fd\bar{3}m$ (Origin Choice 2), $Z = 8$

		model 1	model 2	model 3
a (Å)		10.4746(1)	10.4747(1)	10.4748(1)
Bi	atomic site	16d	96g	96h
	x	1/2	0.4831(2)	0
	y	1/2	0.5180(4)	0.2318(2)
	z	1/2	0.5180(4)	0.7682(2)
	U_{iso} (Å^2)	0.0510(3)	0.012(1)	0.023(1)
	frac	1.0	1/6	1/6
Tc	atomic site	16c	16c	16c
	x	0	0	0
	y	0	0	0
	z	0	0	0
	U_{iso} (Å^2)	0.0014(2)	0.0014(1)	0.0019(2)
O	atomic site	48f	48f	48f
	x	0.3248(1)	0.3248(1)	0.3249(1)
	y	1/8	1/8	1/8
	z	1/8	1/8	1/8
	U_{iso} (Å^2)	0.020[a]	0.197[b]	0.197[c]
O′	atomic site	8b	8b	32e
	x	3/8	3/8	0.385(2)
	y	3/8	3/8	0.385(2)
	z	3/8	3/8	0.385(2)
	U_{iso} (Å^2)	0.031(1)	0.040(1)	0.030(5)
	frac	0.86(1)	0.86(1)	0.215(2)
χ^2		4.207	3.771	3.809
R_{wp}%		3.21	3.04	3.05

[a] $U_{11} = 0.0220(4)$, $U_{22=33} = 0.0198(2)$, $U_{23} = 0.0011(4)$. [b] $U_{11} = 0.0270(4)$, $U_{22=33} = 0.0171(2)$, $U_{23} = 0.0048(3)$. [c] $U_{11} = 0.0250(1)$, $U_{22=33} = 0.0171(3)$, $U_{23} = 0.0051(4)$.

3.2. Neutron Powder Diffraction. Using the *GSAS* software package,[29] the crystal structures of $Bi_2Tc_2O_7$ and Bi_3TcO_8 were refined with both low and room-temperature NPD data. The neutron scattering length of 6.00 fm was used for ^{99}Tc as determined previously.[18] For the bismuth and oxygen atoms, the values listed in a standard table of neutron scattering lengths[30] were employed.

Starting with the ideal pyrochlore structure, space group $Fd\bar{3}m$ (origin choice 2), Rietveld refinement with the room-temperature NPD data of $Bi_2Tc_2O_7$ converged to the structural parameters given in model 1 of Table 1. Within this model, all of the atoms reside in special positions except for the oxygen atom, which has one refinable fractional coordinate. In addition, an oxygen stoichiometry of 6.86(1) was obtained with vacancies only on the O′ atom site (model 1 of Table 1). The calculated density from the NPD results was 8.3892(2) g/cm^3, and the agreement between the observed and calculated NPD patterns is shown in Figure 2. No crystallographic phase transition was observed between

(22) Becke, A. D.; Edgecombe, K. E. *J. Chem. Phys.* **1990**, *92*, 5397.
(23) Silvi, B.; Savin, A. *Nature* **1994**, *371*, 683.
(24) Seshadri, R. *Solid State Sci.* **2006**, *8*, 259–266.
(25) Jepsen, O.; Andersen, O. K. *The Stuttgart TB-LMTO-ASA Program, version 47*; MPI für Festkörperforschung: Stuttgart, Germany, 2000.
(26) Ravel, B.; Newville, M. *J. Synchrotron Rad.* **2005**, *12*, 537.
(27) Poineau, F. Ph.D. Thesis, Université de Nantes: Nantes, France, 2004.
(28) Allen, P. G.; Siemering, G. S.; Shuh, D. K.; Bucher, J. J.; Edelstein, N. M.; Langton, C. A.; Clark, S. B.; Reich, T.; Denecke, M. A. *Radiochim. Acta* **1997**, *76*, 77–86.
(29) Larson, A. C.; Von Dreele, R. B. *General Structure Analysis System (GSAS), Technical Report*, Los Alamos National Laboratory Report, LAUR 86−748, 2004.
(30) Dianoux, A.-J.; Lander, G. *Neutron Data Booklet; OCP Science*: Institut Laue-Langevin: Grenoble, France, 2003.

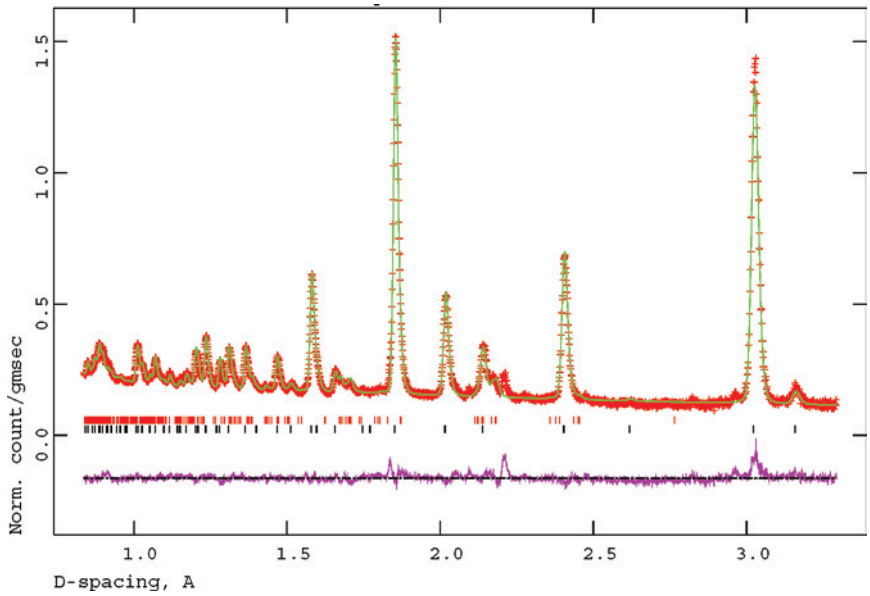

Figure 2. The observed and calculated (model 1 of Table 1) neutron powder profiles for $Bi_2Tc_2O_7$ with the difference curve below. Upper tickmarks represent the TcO_2 impurity (approximately 3.14(5) wt. %) and lower tickmarks the $Bi_2Tc_2O_7$ phase. The powder pattern was obtained on the HIPD instrument.

Table 2. Selected Interatomic Distances (Angstroms) and Angles (Degrees) in $Bi_2Tc_2O_7$ from Room Temperature Neutron Data (Model 1)[a]

Tc−O (× 6)	2.0108(3)
O−Tc−O	94.80(2)
O−Tc−O	85.20(2)
O−Tc−O	180.0
Tc−O−Tc	134.109(4)
Bi−O′(× 2)	2.26781(2)
Bi−O (× 6)	2.6067(5)
O′−Bi−O′	109.471(1)
Bi−O′−Bi	180.0

[a] Standard uncertainties are shown in parentheses.

15 and 300 K. Selected interatomic distances from model 1 are presented in Table 2. Whereas all of the Tc−O bonds are equal, differences in the O−Tc−O bond angles show that the local geometry around technetium is more accurately described as a trigonal antiprism rather than a regular octahedron, which is a special trigonal antiprism geometry.

Ordering of the oxygen vacancies on the O′ site has to be discounted because this would lead to superlattice peaks in the powder diffraction patterns;[31] all of the NPD and XRD Bragg peaks could be indexed. However, the room-temperature results show anomalously large atomic displacement parameters for the bismuth and O′ atoms, indicative of static disorder of the bismuth atom's position and the O′ vacancies. Previous time-of-flight neutron studies successfully modeled static disorder of the bismuth site in $Bi_2Sn_2O_7$,[32] $Bi_2Ru_2O_7$,[33] and various high dielectic materials.[34,35] In our NPD study, we employ a similar methodology.

(31) Beyerlein, R. A.; Horowitz, H. S.; Longo, J. M.; Leonwicz, M. E.; Jorgensen, J. D.; Rotella, F. J. *J. Solid State Chem.* **1984**, *51*, 253–265.
(32) Jones, R. H.; Knight, K. S. *J. Chem. Soc., Dalton Trans.* **1997**, *15*, 2551–2555.
(33) Avdeev, M.; Haas, M. K.; Jorgensen, J. D.; Cava, R. J. *J. Solid State Chem.* **2002**, *169*, 24–34.
(34) Levin, I.; Amos, T. G.; Nino, J. C.; Vanderah, T. A.; Randall, C. A.; Lanagan, M. T. *J. Solid State Chem.* **2002**, *168*, 69–75.
(35) Melot, B.; Rodriguez, E.; Proffen, T.; Hayward, M. A.; Sesahdri, R. *Mater. Res. Bull.* **2006**, *41*, 961–966.

Table 3. Structural Parameters with Standard Uncertainties Shown in Parentheses for Bi_3TcO_8, Space Group $P2_13$, $a = 11.5749(1)$ Å, $Z = 8$

	site	x	y	z
Tc(1)[a]	4a	0.1203(1)	0.1203(1)	0.1203(1)
Tc(2)[a]	4a	0.6175(1)	0.6175(1)	0.6175(1)
Bi(1)[b]	12b	0.1473(2)	0.3545(2)	0.3869(2)
Bi(2)[b]	12b	0.1206(2)	0.1520(2)	0.6290(2)
O(1)[c]	4a	0.0322(4)	0.0322(4)	0.0322(4)
O(2)[c]	4a	0.5319(4)	0.5319(4)	0.5319(4)
O(3)[c]	12b	0.1409(3)	0.2521(3)	0.0569(3)
O(4)[c]	12b	0.6209(3)	0.7575(3)	0.5700(3)
O(5)[c]	4a	0.2891(4)	0.2891(4)	0.2891(4)
O(6)[c]	4a	0.7842(4)	0.7842(4)	0.7842(4)
O(7)[c]	12b	0.2351(3)	0.2130(2)	0.4915(4)
O(8)[c]	12b	0.2596(4)	0.5386(2)	0.0020(4)

[a] Technetium $U_{iso} = 0.0115(4)$ Å^2. [b] Bismuth $U_{iso} = 0.0126(1)$ Å^2. [c] Oxygen $U_{iso} = 0.0257(2)$ Å^2. An R_{wp} of 1.57% and χ^2 of 4.005 was obtained from the structural refinement.

To simulate static disorder of the bismuth atoms in $Bi_2Tc_2O_{7-\delta}$, two additional structural models were explored. Model 2 displaces the bismuth atom from the 16d site (3*m* symmetry) to the 96g site (mirror symmetry) with a diminished occupancy of $^1/_6$. Model 3 displaces the bismuth atom from the 16d site to the 96h site (2-fold symmetry) and the O′ atom from the 8b site ($\bar{4}3m$ symmetry) to the 32e site (3*m* symmetry). In both cases, this atom splitting of the sites decreased the values for R_{wp} and χ^2 from model 1 (Table 1). The U_{iso} values for the bismuth and O′ atoms were also decreased. With current powder diffraction data, model 3 is not preferred over model 2 or vice versa, but both more accurately describe the local structure than the ideal pyrochlore structure (model 1).

The structure of Bi_3ReO_8[16] was used as a starting model for refinement with the Bi_3TcO_8 NPD data. The refinement converged to the parameters listed in Table 3 with a cubic lattice, $a = 11.5749(1)$ Å, space group $P2_13$. The data were collected with a high-resolution neutron diffractometer because the number of refinable structural parameters was 29 in Bi_3TcO_8. In comparison, just 5 structural parameters

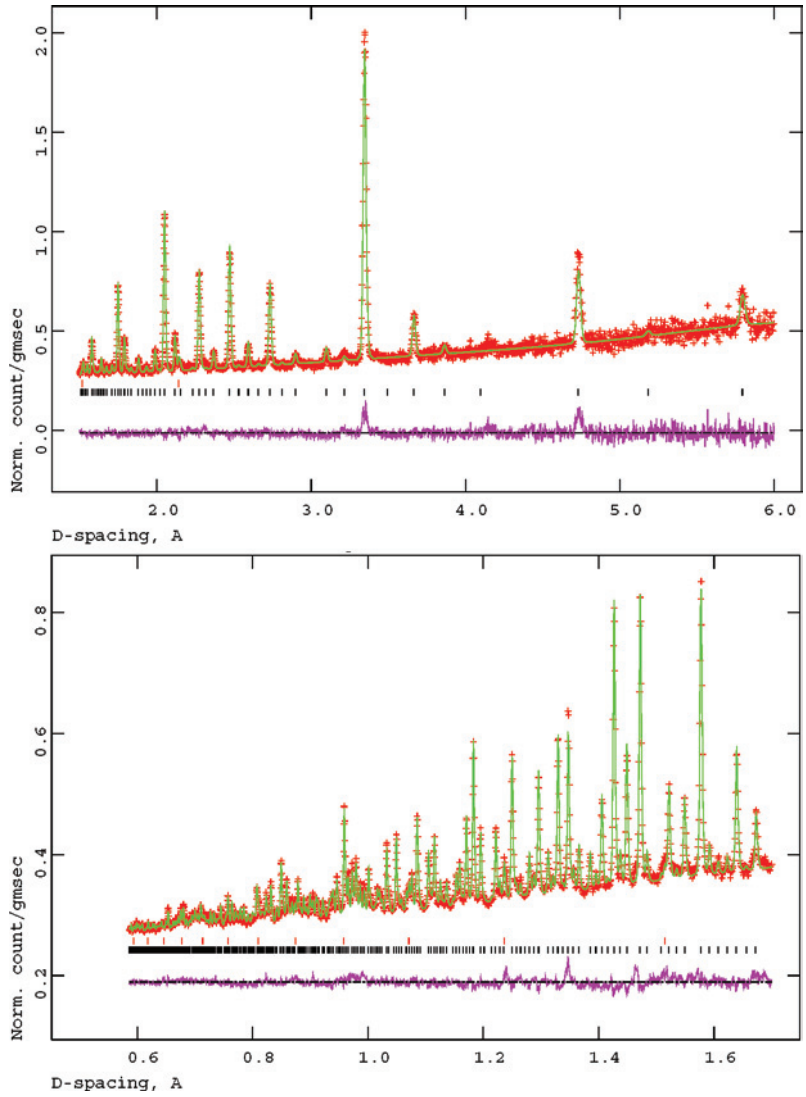

Figure 3. The observed and calculated (Table 4) neutron powder profiles for Bi_3TcO_8 with the difference curve shown below. The powder patterns were obtained at the NPDF instrument and are shown for the higher *d*-spacing bank in the top panel and lower *d*-spacing bank in the bottom panel. Upper tickmarks represent the vanadium container and lower tickmarks the Bi_3TcO_8 phase.

Table 4. Selected Interatomic Distances (Angstroms) and Angles (Degrees) in Bi_3TcO_8 from Room-Temperature Neutron Data[a]

Tc(1)−O(1)	1.767(9)	Tc(2)−O(2)	1.717(9)
Tc(1)−O(3) × 3	1.711(4)	Tc(2)−O(4) × 3	1.713(4)
O(1)−Tc(1)−O(3)	110.3(2)	O(2)−Tc(2)−O(4)	112.0(1)
O(3)−Tc(1)−O(3)	108.6(2)	O(4)−Tc(2)−O(4)	106.8(2)
Bi(1)−O(4)	2.945(4)	Bi(2)−O(3)	2.837(4)
Bi(1)−O(5)	2.135(2)	Bi(2)−O(6)	2.139(2)
Bi(1)−O(7)	2.278(4)	Bi(2)−O(7)	2.190(5)
Bi(1)−O(7)	2.490(5)	Bi(2)−O(7)	2.702(3)
Bi(1)−O(8)	2.671(4)	Bi(2)−O(8)	2.131(5)
Bi(1)−O(8)	2.117(5)	Bi(2)−O(8)	2.979(4)
Bi(1)−O(1)	3.074(4)	Bi(2)−O(2)	3.012(4)
Bi(1)−O(3)	3.108(4)	Bi(2)−O(4)	3.361(4)

[a] Standard uncertainties are shown in parentheses.

were refined in $Bi_2Tc_2O_7$ (model 1). Because of the large amount of refinable parameters in Bi_3TcO_8, all of the U_{iso}'s were constrained to one value for each atom type. The calculated denstiy from the NPD results was 7.2924(1) g/cm^3, and the agreement between the observed and calculated profiles is shown in Figure 3. Selected distances and angles are presented in Table 4. No crystallographic phase transition was observed between 15 and 300 K.

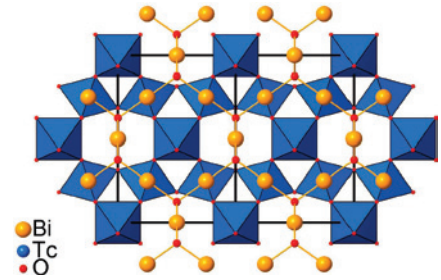

Figure 4. The structure of the pyrochlore structure ($Bi_2Tc_2O_7$) viewed down the [110] direction of the cubic cell. The Tc_2O_6 network is represented by cornersharing octahedra whereas the Bi_2O' network by the ball-and-stick model.

4. Discussion

4.1. $Bi_2Tc_2O_7$. Pyrochlore oxides have the general formula $A_2B_2O_6O'$, and the structure consists of two interpenetrating networks.[36] The B_2O_6 sublattice consists of corner-sharing BO_6 octahedra, whereas the A_2O' sublattice consists of corner-sharing $O'A_4$ tetrahedra (Figure 4). This topology can accommodate a variety of substitutions for both the A and

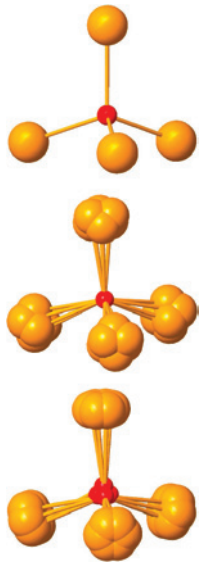

Figure 5. O′Bi_4 tetrahedra for model 1 (top), model 2 (middle), and model 3 (bottom). The split yellow atoms represent the displacement of the bismuth atoms from their average position in the cubic crystal.

B cation sites resulting in a plethora of chemical compounds.[37]

In addition to its versatility for cationic substitution, the pyrochlore structure can also accommodate both cationic and anionic vacancies on the A_2O' sublattice. Oxygen vacancies often occur when the A cation has a lone pair of electrons, which can form hybridized states with the virtual energy levels of the oxygen vacancies.[37] These hybridized states stabilize the pyrochlore structure despite an increase in the electrostatic repulsion between the unscreened A cations.

An ordering of the oxygen vacancies can also occur as in $Pb_2Ru_2O_{6.5}$,[31] or they can be disordered throughout the crystal as in $Bi_2Ru_2O_{7-\delta}$.[33] Oxygen vacancies in pyrochlore oxides are important because they can have a significant impact on the materials properties. They can drive semiconductor-to-metal transitions as in neodymium-doped bismuth ruthenates,[38] or strongly influence the dielectric properties as in the bismuth niobates and tantalates.[35] As evident from the NPD analysis, the oxygen vacancies in $Bi_2Tc_2O_{7-\delta}$ are disordered throughout the crystal and occur only on the Bi_2O' sublattice.

Also relevant to the structure is the stereochemical activity of the bismuth lone-pair electrons. The O′Bi_4 tetrahedra from three models presented in the Results section (Figure 5) illustrate the positions of the bismuth and O′ atoms, which are split in models 2 and 3. Whereas powder diffraction cannot provide enough information to choose between models 2 and 3, the NPD data does show the existence of static disorder of the bismuth cation's position from its average location. These structural features are due to the inert pair effect of the bismuth $6s^2$ electrons, which displace the bismuth atoms from its centrosymmetric position. Indeed, the electronic localization function (ELF) calculations further illustrate this point. The valence ELF of $Bi_2Tc_2O_7$ is plotted

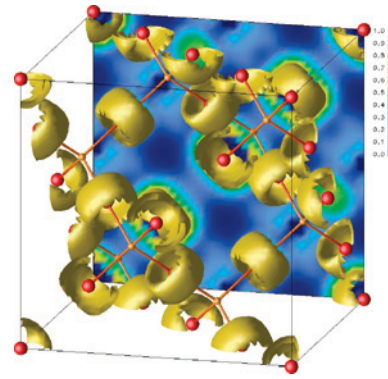

Figure 6. Representation of the isosurfaces for the ELF projected within the unit cell of $Bi_2Tc_2O_7$ with a value of 0.65 for the ELF. The red atoms represent the bismuth cations and the yellow atoms the O′ anions. The back plane of the cell also displays the ELF as a map running from deep blue (poorly localized) to white (strongly localized). The technetium and oxygen atoms are not shown for clarity.

within the real space of the crystal structure (model 1) in Figure 6 with the technetium and oxygen atoms not displayed for clarity. The isosurfaces of the ELF for a value of 0.65 are displayed as ringlike lobes around the bismuth cations. Because the bismuth atoms are in a special position (16d, model 1), the $6s^2$ lone-pair electrons are forced by the $3m$ symmetry of that site to be manifested as symmetric rings. Otherwise, they would be localized asymmetrically around the bismuth site albeit in an incoherent manner. The bismuth atom's position would consequently be shifted from their special position in an equally incoherent manner.

On the basis of its striking structural similarity to $Bi_2Ru_2O_7$ and $Pb_2Ru_2O_{6.5}$, $Bi_2Tc_2O_7$ should have materials properties similar to those of its ruthenium congeners. These pyrochlore ruthenates are classified as metallic oxides with Pauli paramagnetism.[39] In $Bi_2Ru_2O_7$ and $Pb_2Ru_2O_{6.5}$, the Ru−O−Ru bond angles are relatively open for a pyrochlore-type structure, 133° in the former[33] and 135° in the latter.[31] The wider angles allow greater covalency between the metal d states and oxygen p states and could give rise to metallicity.[40–42] Indeed, the pyrochlores $Ln_2Ru_2O_7$ (Ln = lanthanide) have all been found to be insulating due to the smaller A cation radius and therefore narrower Ru−O−Ru bond angle.[38,43–45] In $Bi_2Tc_2O_{7-\delta}$, the Tc−O−Tc bond angle was found to be 134.125(4)°, which is close to that of the metallic pyrochlore ruthenates. The band-structure calculations performed in the present study predict metallic conductivity in $Bi_2Tc_2O_7$ and further support the position that covalency between the metal d states and oxygen p states is chiefly responsible. The LMTO densities of states (DOS) are displayed in the top panel of Figure 7. The narrow bismuth

(36) Sleight, A. W. *Inorg. Chem.* **1968**, *7*, 1704–1708.
(37) Subramanian, M. A.; Aravamudan, G.; Subba Rao, G. V. *Prog. Solid State Chem.* **1983**, *15*, 55–143.
(38) Field, M.; Kennedy, B. J.; Hunter, B. A. *J. Solid State Chem.* **2000**, *151*, 25–30.
(39) Tachibana, M.; Kohama, Y.; Shimoyama, T.; Harada, A.; Taniyama, T.; Itoh, M.; Kawaji, H.; Atake, T. *Phys. Rev. B* **2006**, *73*−1–4.
(40) Kanno, R.; Takeda, Y.; Yamamoto, T.; Kawamoto, Y.; Yamamoto, O. *J. Sol. State Chem.* **1993**, *102*, 106–114.
(41) Kennedy, B. J. *J. Solid State Chem.* **1995**, *119*, 254–259.
(42) Lee, K.-S.; Seo, D.-K.; Whangbo, M.-H. *J. Solid State Chem.* **1997**, *131*, 405–408.
(43) Kennedy, B. J.; Vogt, T. *J. Solid State Chem.* **1996**, *126*, 261–270.
(44) Yamamoto, T.; Kanno, R.; Takeda, Y.; Yamamoto, O.; Kawamoto, Y.; Takano, M. *J. Solid State Chem.* **1994**, *109*, 372–383.
(45) Taira, N.; Wakeshima, M.; Hinatsu, Y. *J. Mater. Chem.* **2002**, *12*, 1475–1479.

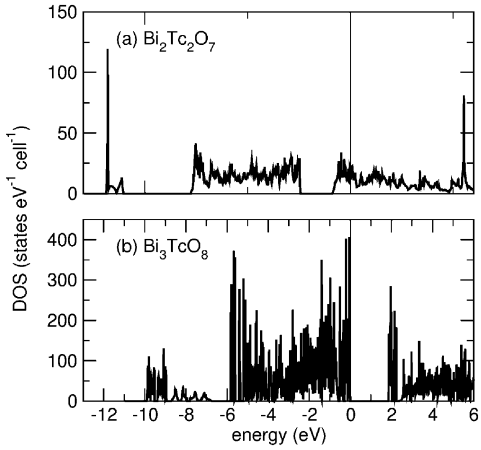

Figure 7. The calculated density of states for (a) $Bi_2Tc_2O_7$ and (b) Bi_3TcO_8. The origin of the energy axis is the Fermi level, represented by the solid vertical line.

s states are shown to be at an energy around −11 eV below the Fermi level. The conduction band seems to consist primarily of low-spin technetium t_{2g} states mixed with the antibonding oxygen p states. This covalency is predicted by the structural details obtained from the neutron results and seems to be a consequence of a short Tc−O bond and a relatively open Tc−O−Tc bond angle.

However, the M−O−M bond angle does not seem to be the sole qualifier in determining transport properties in pyrochlore oxides. For example, $Bi_2Rh_2O_{7-\delta}$ is a metallic oxide despite a narrow Rh−O−Rh bond angle of 130.1°.[46] The role of oxygen stoichiometry and lone pair electrons on the A cation site seem to be just as critical as the M−O−M bond angle. Oxygen sub-stoichiometry is present in all three $Bi_2M_2O_7$ pyrochlores: 6.92 for ruthenium,[33] 6.8 for rhodium,[46,47] and 6.86(1) for technetium. Although the role of oxygen vacancies in metallic conductivity has yet to be quantified, several studies have attempted to explain the observed conduction through band structure arguments. Some studies assert the importance of the s states of the bismuth cations[48] mixing with the ruthenium d states (t_{2g}), whereas more recent ones emphasize the empty p states of bismuth hybridizing with the ruthenium d states.[49,50]

Whatever the real reason for the metallicity in $Bi_2Ru_2O_{7-\delta}$ and $Pb_2Ru_2O_{6.5}$, these materials are also remarkable for their chemical properties. Combined with their impressive electrical conductivity, catalytic activity has also been observed in these ruthenates;[9] thus, their use as electrodes in the reduction and evolution of oxygen.[7,10] Similarly, $Bi_2Tc_2O_{7-\delta}$ could exhibit both properties, making it an interesting candidate for a specialized, technological application of ^{99}Tc. Overall, the structural information from the NPD data of $Bi_2Tc_2O_{7-\delta}$ strongly suggests metallic conductivity based on the structural information of related oxides.

(46) Kennedy, B. J. *Mater. Res. Bull.* **1997**, *32*, 479–483.
(47) Longo, J. M.; Raccah, P. M.; Kafalas, J. A.; Pierce, J. W. *Mater. Res. Bull.* **1972**, *7*, 137–146.
(48) Cox, P. A.; Goodenough, J. B.; Tavener, P. J.; Telles, D.; Egdell, R. G. *J. Solid State Chem.* **1986**, *62*, 360–370.
(49) Hsu, W. Y.; Kasowski, R. V.; Miller, T.; Chiang, T.-C. *Appl. Phys. Lett.* **1988**, *52*, 792–794.
(50) Ishii, F.; Oguchi, T. *J. Phys. Soc. Jpn.* **2000**, *69*, 526–531.

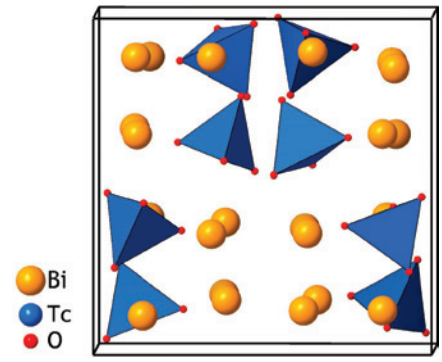

Figure 8. The cubic cell of Bi_3TcO_8 viewed down the [100] direction. The oxygen atoms not part of the TcO_4 tetrahedra are not shown for clarity.

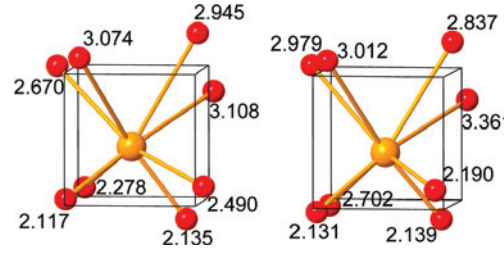

Figure 9. The oxygen coordination around the Bi(1) (left) and Bi(2) (right) cations in Bi_3TcO_8. The corners of the cube drawn around the central bismuth atom represent the anion positions in the ideal fluorite structure and interatomic distances are in angstroms.

4.2. Bi_3TcO_8. The structure of Bi_3ReO_8 is unique and can be described as that of a distorted fluorite with a doubled cubic unit cell.[16] Like CaF_2, it also has a cation/anion ratio of 1:2 and unlike the A_3ReO_8 (A = Y, lanthanide) compounds[51,52] the Re(VII) cations are not octahedrally coordinated. The chief reason for the distortion of the ideal flourite structure is the formation of ReO_4 tetrahedra and the displacement of bismuth due to the lone pair effect. Bi_3TcO_8 is isostructural to Bi_3ReO_8. As shown in Figure 8, Bi_3TcO_8 contains an ordered array of TcO_4 tetrahedra aligned to one of the ⟨111⟩ directions of the cubic cell. The TcO_4 tetrahedra are not ideal (Table 4) as in the pertechnetate anion but they are close enough to exhibit a similar pre-edge feature in the XANES spectrum as that of the TcO_4^- anion. The bismuth lone-pair effect can also be observed in the open coordination around the bismuth cations as shown in Figure 9. As done for $Bi_2Tc_2O_7$, ELF calculations performed for Bi_3TcO_8 map out the location of the Bi $6s^2$ lone pair electrons. Figure 10 displays the isosurfaces of the ELF for a value of 0.80 and is consistent with the predicted location of the lone pair from Figure 9.

Interestingly, whereas Bi_3ReO_8 is the predominant phase in the Bi−Re−O system under nonoxidizing conditions, the predominant phase in the Bi−Tc−O system is $Bi_2Tc_2O_7$ and not Bi_3TcO_8. When reactions between ReO_2 and Bi_2O_3 were carried out in evacuated quartz ampoules, the Re(IV) cations were oxidized to form Bi_3ReO_8 with some residual impurities (bismuth metal and other phases).[14] When the same reactions

(51) Baud, G.; Besse, J. P.; Chevalier, R. *J. Solid State Chem.* **1979**, *29*, 267–272.
(52) Rae-Smith, A. R.; Cheetham, A. K.; Fuess, H. *Z. Anorg. Allg. Chem.* **1984**, *510*, 46–50.

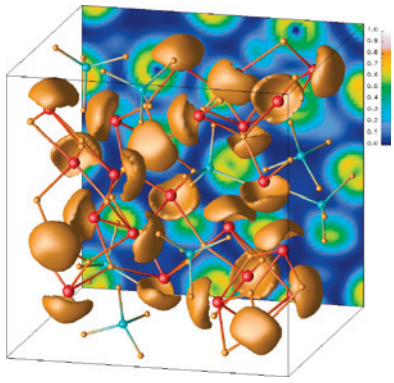

Figure 10. Representation of the isosurfaces for the ELF with a value of 0.8 projected within the unit cell of Bi_3TcO_8. The red atoms represent the bismuth cations, the blue the technetium cations, and the yellow the oxygen anions. The back plane of the cell also displays the ELF as a map running from deep blue (poorly localized) to white (strongly localized).

were performed with TcO_2, the Tc(IV) cations remained in the same oxidation state to form the pyrochlore phase. This observation fits well with known periodic trends; higher oxidation states in transition metals become more stable for the heavier members of a group (i.e., $Re^{+7} > Tc^{+7} > Mn^{+7}$).

Unlike the $Bi_2Tc_2O_7$ compound, Bi_3TcO_8 is expected to be an insulator. Technetium is fully oxidized and the Bi $6s^2$ electrons appear to be completely isolated from each other. The electronic band structure calculations of Bi_3TcO_8 further support this claim (bottom panel of Figure 7). Whereas the transport properties may be uninteresting, the compound could have attractive catalytic properties. For example, the bismuth molybdates containing Mo^{6+} cations have been widely studied for the partial oxidation of C_3 hyrdrocarbons.[53] Similarly, the Tc^{7+} cations could have interesting catalytic properties.

Although the ternary oxides containing rhenium do not appear to have significant catalytic activity,[54] one interesting property of Bi_3ReO_8 is its high melting point. Instead of decomposing below 400 °C like the A_3ReO_8 (A = Y, Tb−Lu) compounds,[55] Bi_3ReO_8 melts congruently at around 1473 °C.[14] No doubt, this is a consequence of its fluorite-type structure. Ionic crystals with the fluorite structure have a high lattice energy due to the high Madalung constant of this structure type.[56] This could be expected in Bi_3TcO_8, which could make it an attractive candidate as a stable waste form for ^{99}Tc.

4.3. $Bi_3Tc_3O_{11}$. The stoichiometry of this phase remains speculative because the compound was not obtained monophasically. XRD powder patterns suggest the third phase is $Bi_3Tc_3O_{11}$ based upon the closeness of its cubic lattice (a = 9.3433(1) Å) and the lattice parameter of $Bi_3Ru_3O_{11}$ (a = 9.3050(2) Å).[57] The structure of $Bi_3Ru_3O_{11}$ can be described as a $KSbO_3$-type structure with edge-sharing Ru_2O_{10} octahedral units.[57] One striking feature about this structure is the metal−metal bonding across the shared edge. When the structural parameters from $Bi_3Ru_3O_{11}$ were used with the measured lattice of the technetium analogue, a Tc−Tc interatomic distances of 2.61 Å was calculated. The XRD powder pattern of $Bi_3Tc_3O_{11}$ with Bi_3TcO_8 and the 2θ listing of Bragg peaks for $Bi_3Tc_3O_{11}$ can be found in the Supporting Information file.

5. Conclusions and Future Work

Two new compounds of a new ternary system were prepared. NPD results confirm the stoichiometries of the new compounds to be $Bi_2Tc_2O_{7-\delta}$ and Bi_3TcO_8. XANES spectra indicate the local environment of technetium to be tetrahedral in one and centrosymmetric in the other. In addition, the structural studies using NPD data reveal some interesting structural features, which are expected to strongly influence the materials properties. For example, $Bi_2Tc_2O_{7-\delta}$ is expected to be a metallic oxide based on (1) its relativetly open Tc−O−Tc bond angle, (2) oxygen substoichiometry, and (3) disorder of the bismuth cation site. For Bi_3TcO_8, we expect a high melting-point oxide with possible catalytic activity due to the Tc^{7+} species. In addition, electronic band structure calculations further strengthen the simple structural and valence arguments for predicting $Bi_2Tc_2O_7$ to be a metal and Bi_3TcO_8 an insulator.

Future work includes transport and magnetic susceptibility measurements for $Bi_2Tc_2O_{7-\delta}$ and chemical activity measurements for Bi_3TcO_8. In the case of $Bi_2Tc_2O_{7-\delta}$, confirmation that it exhibits metallic conductivity and Pauli paramagnetism could help further clarify the role of oxygen vacancies and large cations with lone-pair electrons such as bismuth in the transport properties of pyrochlore oxides. For Bi_3TcO_8, solubility measurements and thermogravimetric studies could determine its suitability as a stable waste form. This study and future studies on these materials could open up a new chapter on the materials chemistry of mixed-metal technetates, a potentially important class of oxides yet to be explored.

Acknowledgment. This work has benefited from the use of NPDF and HIPD at the Lujan Center at the Los Alamos Neutron Science Center, funded by DOE Office of Basic Energy Sciences. Los Alamos National Laboratory is operated by Los Alamos National Security LLC under DOE Contract DE-AC52-06NA25396. The upgrade of NPDF has been funded by NSF through grant DMR 00-76488. Use of the Advanced Photon Source was supported by the U.S. Department of Energy, Office of Science, Office of Basic Energy Sciences, under Contract No. DE-AC02-06CH11357. We would also like to thank Carol J. Burns from Los Alamos National Laboratory for supplying us with the pertechnetate salt.

Supporting Information Available: The XRD powder pattern of mixed $Bi_3Tc_3O_{11}$ and Bi_3TcO_8 phases with 2θ list of the Bragg peaks belonging to $Bi_3Tc_3O_{11}$. Crystallographic information files including neutron powder data for $Bi_2Tc_2O_7$ and Bi_3TcO_8. This material is available free of charge via the Internet at http://pubs.acs.org.

IC8003273

(53) Bettahar, M. M.; Costentin, G.; Savary, L.; Lavalley, J. C. *Appl. Catal., A* **1996**, *145*, 1–48.
(54) Rae-Smith, A. R. Ph.D Thesis, Oxford University: Oxford, U.K., 1979.
(55) Baud, G.; Besse, J. P. *Mater. Res. Bull.* **1974**, *9*, 1499–1502.
(56) West, A. R. *Basic Solid State Chemistry*; John Wiley & Sons Ltd: Chichester, England, 2nd ed., 1999.
(57) Facer, G. R.; Elcombe, M. M.; Kennedy, B. J. *Aust. J. Chem.* **1993**, *46*, 1997–1907.